Effects of topography and multi-asperity contacts on nano-scale elastic property measurements by atomic force acoustic microscopy

Gheorghe Stan[1] and Robert F. Cook

Ceramics Division, Materials Science and Engineering Laboratory,
National Institute of Standards and Technology, Gaithersburg, Maryland 20899, USA

Abstract. Endowed with nano-scale spatial resolution, atomic force acoustic microscopy (AFAM) provides extremely localized elastic property measurements. We advance here the applicability of AFAM for obtaining accurate elastic modulus measurements on surfaces with nano-size features by considering the topography contribution to the AFAM signal. On nano-size granular Au films, the elastic modulus at the grain scale has been mapped out by deconvoluting the contact geometry effect in the AFAM image. Significant variation in the contact area over granular topography arises as the probe is either in single- or multiple-asperity contact with the surface. By correlating the AFAM and topography images we determine variations in the elastic modulus with a lateral resolution better than 10 nm.

Keywords: thin films, nano-elasticity, atomic force acoustic microscopy
PACS: 68.35.Gy

INTRODUCTION

Next-generation electronic devices, based on micro- and nano-electromechanical systems [1] (MEMS and NEMS), employ accurate knowledge and control of both mechanical and electrical properties of materials at ultra-small scales. As the size of device elements is reduced further and further down to the nano scale, material properties (e.g., mechanical and electrical) can exhibit significant variations from those of their bulk counterparts due to the change in the surface-to-volume ratio. The inherent effects due to the proximate surface alter the properties of the reduced-scale constituents (e.g., crystallites) and modify the mechanical response of the microstructure as a whole [2, 3]. For some particular geometries it is possible to deduce the response of the nano-sized constituents by testing the assembly at the macro-scale [4, 5]. However, it is obviously more desirable to directly measure the local material properties of a microstructure [6].

Instrumentation developed for nano-scale characterization, such as atomic force microscopy (AFM), enables access at this scale but the challenge is to extract and quantify material properties in such measurements. It is also desirable to make a non-destructive and in situ characterization of nano-structured assemblies. These needs can be addressed by expanding the capabilities of AFM techniques to provide local property measurements based on accurate knowledge of the interaction between the testing probe and the investigated structure.

In this paper we have investigated the local elastic response of nano-grained Au thin films and propose a methodology to extract the elastic modulus of material surfaces that exhibit nano-scale topographic features. Contact area variations have been tracked as the probe is in either in single- or multiple-asperity contact with the granular surface. This variation is then deconvoluted from the AFAM signal at every point in the scan. The elastic modulus is obtained as a local average within 10 nm lateral resolution. Although the interpretation of these measurements is more complicated than those on individual manufactured small volumes, such as pillars [7] or pyramids [8], the goal is to develop a technique suitable for measuring *in situ* nano-structured assemblies such as those in MEMS and NEMS.

EXPERIMENTAL MEASUREMENTS

Continuous, 100 nm thick Au films were fabricated by electrodeposition on Si (100) wafers. For adhesion purposes, a preliminary 2 nm thick Ti layer was deposited on the Si before the Au. (For the present work only the 100 nm thick films have been fully investigated but the technique is suitable for thinner films as well.) A well-defined grain structure with grains between 60 nm and 90 nm in size was revealed by scanning tunneling microscopy (STM). The peak-to-valley height in the scanned areas was no larger than 15 nm.

The elastic response of the granular film was mapped out over 1 μm^2 areas by tracking the change in the

[1] Corresponding author, email: gheorghe.stan@nist.gov

CP931, *Frontiers of Characterization and Metrology for Nanoelectronics,*
edited by D. G. Seiler, A. C. Diebold, R. McDonald, C. M. Garner, D. Herr, R. P. Khosla, and E. M. Secula
© 2007 American Institute of Physics 978-0-7354-0441-0/07/$23.00

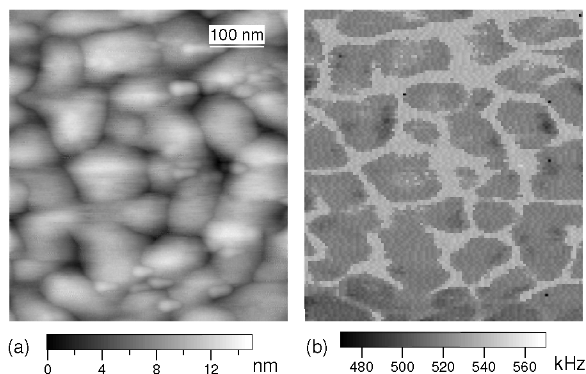

FIGURE 1. (a) AFM topography of a 100 nm thick Au film; (b) the first contact resonance frequency over the area shown in (a).

resonance frequency of an AFM probe during contact scanning. The technique, commonly called atomic force acoustic microscopy [9, 10] (AFAM), consists of monitoring how the resonance frequency of the cantilever changes when the AFM probe is brought, from air, into contact with the investigated material. Excited by a superimposed small-amplitude vibration, the contact behaves like a linear-elastic spring and the shift in the resonance frequency provides a quantification of the elastic modulus of the contacted region.

Figure 1 shows a 520 nm x 630 nm area of the 100 nm thick Au film successively scanned in AFM tapping mode and AFAM. For AFAM-imaging complementary software (LabView, National Instruments, Austin TX) to AFM instrumentation (MultiMode, Veeco, Santa Barbara, CA) has been developed [11]. In this setup the modulation (about 0.5 nm amplitude) is applied through the piezoelectric element located beneath the cantilever's base. Both the excitation and the detection are made with the same lock-in amplifier (Model 7280, Signal Recovery, Oak Ridge, TN). Once a contact resonance is identified (e.g., the first contact resonance, as shown in Fig. 1(b)), an AFAM image is made by scanning over the designated area and, at every point in the scan, the frequency spectrum around that resonance frequency is recorded [12]. Thus, at every location, a 100 kHz frequency sweep in steps of 500 Hz is performed in 200 ms. Later on, the contact resonance frequency is identified in the recorded spectrum and used to construct the AFAM image. The LabView instrumentation is used to perform scan and acquisition at every point, along with maintaining active AFM amplitude feed-back in order to assure a constant low-frequency deflection of the AFM probe during the scan.

As observed by the correspondence between the two images in Fig. 1, the topography and contact resonance

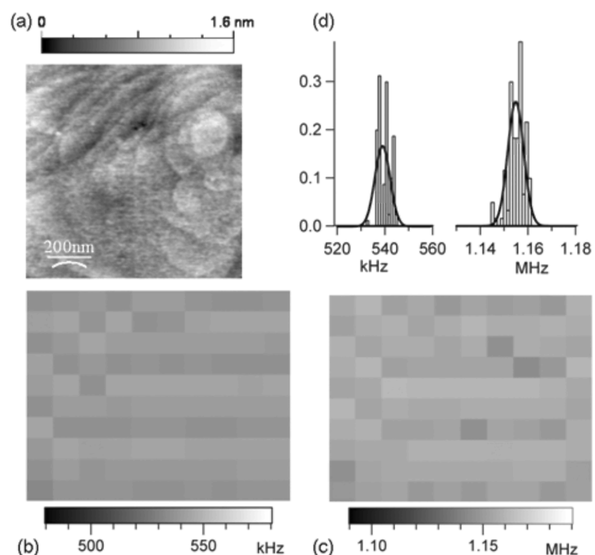

FIGURE 2. (a) AFM topography of the Au reference film; (b) and (c) the first and the second contact resonances over the same area as in (a); (d) histograms of the measurements shown in (b) and (c).

frequency are well correlated. Nominally, a slightly reduction in elastic modulus is expected to occur in intergrain regions as an effect of the mismatch between adjacent grains [3, 13]. Contrarily, in the intergrain regions in Fig. 1, the contact resonance frequency is observed to increase. This is because at the nano-scale, besides the modulation in the elastic modulus due to material properties, the AFAM measurements are also sensitive to topographical features that modify the contact area. Previous works on mapping the elastic behavior at the nano-scale by using AFAM either investigated large areas [14] or ignored any topography-induced artifacts [15].

In terms of the absolute value of the elastic modulus, we have compared the measurements with those made on a reference Au film in the same experimental conditions [16]. The reference was a 300 nm thick Au (111) film epitaxially grown on mica (Georg Albert PVD-Beschichtungen, Heidelberg, Germany). As can be seen in Fig. 2(a) the surface of this reference is essentially flat over a large area. The peak-valley height is only 1.5 nm over a 1 μm^2 area (rms roughness 0.2 nm). In this case, because there are minor changes in the contact area, the measurements were performed in a 10 x 10 grid covering the investigated area. The most probable contact resonance frequencies were then precisely determined by fitting the histograms of the measurements with Gaussian distributions, as is shown in Fig. 2(d) [12]. By using a beam-cantilever model [17], the relative stiffness of the contact along the tip axis is $k^{*}/k_C = 55$, (where the cantilever stiffness is k_C, $f_1^{Au,ref} = 540 \pm 0.5$ kHz

and $f_2^{Au,ref} = 1155 \pm 0.5$ kHz). The two measured contact resonance frequencies on the Au reference film are also used to determine [17] the tip position relative to the length of the cantilever, $\lambda = 0.939$. Knowing λ we need to track only the first contact resonance frequency in order to calculate the contact stiffness on the investigated granular topography.

The effect of the contact area change on the measured contact resonance frequencies becomes even more important in AFAM imaging where we cannot use 1 μm^2-average values but want to detect nano-scale variation in the elastic modulus. In this case we have to trace and consider any change in the contact area during the scan. Until now no corrections for the contact area have been considered in AFAM imaging.

RESULTS AND DISCUSSION

Usually in interpreting AFAM measurements the tip-sample interaction is described as a Hertzian contact between two elastic paraboloids. The contact acts as a spring coupled to the end of the AFM probe; the contact stiffness along the direction perpendicular to the tangential plane of contact is given by [18]

$$k^\star = 2aE^\star, \tag{1}$$

where a is the contact radius, $E^\star = (1/M_T + 1/M_S)^{-1}$ is the reduced elastic modulus, and M_T and M_S are the indentation moduli of the tip and sample, respectively. In the isotropic case, the indentation modulus is simply expressed in terms of the Young's modulus E and Poisson's ratio ν of the material, $M = E/(1-\nu^2)$. However, for anisotropic materials, no simple analytical expression is available for the indentation modulus, and numerical calculation is used [19].

Under a normal applied load, P, the Hertzian contact radius is given by

$$a = \left(\frac{3PR}{4E^\star}\right)^{1/3}, \tag{2}$$

where $R = (1/R_T + 1/R_S)^{-1}$ is the relative curvature at the contact between the tip radius R_T and the sample radius of curvature R_S. When the sample surface is flat R is simply equal with the tip radius R_T. Under the same applied load, successive measurements made on a reference of known indentation modulus, M_R, and a test sample will provide a measure for the indentation modulus M_S of the sample from the contact stiffness ratio:

$$\frac{k_S^\star}{k_R^\star} = \left(\frac{E_S^\star}{E_R^\star}\right)^{2/3} = \left(\frac{M_S}{M_R}\cdot\frac{M_R+M_T}{M_S+M_T}\right)^{2/3}. \tag{3}$$

Using this ratio, determined from the measured contact resonance frequencies on the reference Au(111) film and on top of some relatively flat grains, the indentation modulus of the grains is estimated to be 75 GPa. The indentation modulus of the tip was taken as 165 GPa, appropriate for Si (100) single-crystal [19]. However, to account for the contact area effect in AFAM measurements on the granular surface shown in Fig. 1(a), we have to consider the local change in the curvature of the surface.

To track the change in the radius of curvature, a bidimensional parabolic fit was considered for the topography shown in Fig. 1(a). At every location in the scan, the contact reconstruction between the sample and the tip was performed. The AFM probe used in these measurements was a single-crystal Si (MPP-23100 VeecoProbe, Veeco) with $k_C \sim 35$ N/m. By scanning the AFM probe used against sharp spikes (silicon grating TGT1, NT-MDT, Moscow, Russia), the shape of the probe was determined to be spherical with a radius of approximately 70 nm.

With a spherical AFM probe of radius comparable to the size of grains, the contact on the Au granular surface not only varies in size during a scan but also in the number of contacts. The contact is a single-asperity contact (SAC) on top of the grains whereas between grains the probe could be simultaneously in contact with two or three grains and form a multi-asperity contact (MAC). Considering the grains as asperities with spherical summits of known curvatures, the contact area at a given location is obtained as a summation over the grains contacting the probe at that location [20]:

$$A_c^{MAC} = \sum_i \pi a_i^2 = \pi \sum_i \delta_i R_i, \tag{4}$$

where δ_i is the depth of deformation between the tip and an asperity of radius R_i. In the case of multi-asperity contact, the applied load is distributed between the summits of the asperities that are in contact with the tip

$$P = \frac{4}{3}\sum_i E_i^\star R_i^{1/2}\delta_i^{3/2} \approx \frac{4}{3}\langle E^\star\rangle \sum_i R_i^{1/2}\delta_i^{3/2}. \tag{5}$$

In Eq. (5) $\langle E^\star\rangle$ defines the local average of the reduced elastic modulus at the contact and describes the equivalent elastic response of the asperities forming the contact. The contact stiffness of a multi-asperity contact is then the equivalent stiffness of the parallel-coupled asperities

$$k_{MAC}^\star = 2\langle E^\star\rangle\sqrt{A_c^{MAC}/\pi}, \tag{6}$$

with A_c^{MAC} defined in Eq. (4).

By using the beam-cantilever model [17] the measured contact resonance frequency is converted to the contact stiffness normalized to the cantilever stiffness, $k^\star/k_C$. Thus, to extract $\langle E^\star\rangle$ from Eq. (6) we need either to make

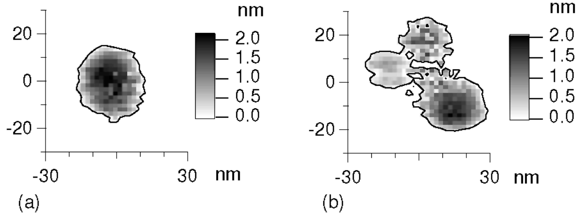

FIGURE 3. (a) On top of a grain the contact is single-asperity contact; (b) within an intergrain region a multi-asperity contact is formed between the probe and the adjacent grains. All the units are in nm.

an accurate calibration for the cantilever stiffness k_C or, more conveniently, to use the ratio of Eqs. (6) and (1):

$$\langle E^{\star}\rangle_{MAC} = E^{\star}_{ref}\frac{k^{\star}_{MAC}}{k^{\star}_{ref}}\sqrt{\frac{A_c^{SAC}}{A_c^{MAC}}}, \tag{7}$$

with $A_c^{SAC} = \pi a^2$ the single-asperity contact area on the flat-surface reference.

The applied load P was maintained, about 2 μN, in the measurements made on both the flat-surface reference Au film and the granular Au film. Equations (4) and (5) were then used to reconstruct the contact area at every location in the scan shown in Fig. 1(a) assuming the Si spherical probe was indenting the granular Au surface under an applied load of 2 μN. At a given location, the compressions δ_i were increased in small increments while the nearest asperities come gradually in contact with the probe. The limit is reached when the total load, distributed over the contacted asperities, equals the applied load of 2 μN. The contact radius on every contacted asperity was then calculated and used in (6) and (7) to obtain $\langle E^{\star}\rangle$ at that location.

Under the same applied load, $P = 2\mu$N, Fig. 3 shows the summit interception at the contact on top of a grain and within an intergrain region where three adjacent grains are in contact with the sample. On top of the grain there is a single-asperity contact characterized by a circular contact area, whereas within the intergrain region the contact area is defined by three adjacent circles. In our calculations we have neglected the overlap of the asperities forming a multi-asperity contact and treated them as individual contacts.

On top of the grain, Fig. 3(a), the probe-sample vertical deformation and the contact radius are larger than in any of the asperities that form the multi-asperity contact in Fig. 3(b). However, the whole contact area is larger in Fig. 3(b). This change in the contact area has to be considered in calculating the elastic modulus from the measured contact stiffness on granular surfaces.

Both the granular Au topography and contact stiffness have been used in solving Eq. (7) for the reduced elastic modulus, $\langle E^{\star}\rangle$. In Fig. 4 are shown the calculated maps for the contact area and the indentation modulus over the scanned area. Qualitatively, the grain delimitation is easily observed in both images and good correlations with the topography and contact resonance frequency scans are identified. Overall, the multi-asperity contacts between grains lead to an increase in the contact area, Fig. 4(a). This in turn is responsible for the measured increase in the contact resonance frequency. However, as can be seen in Fig. 4(b), the elastic modulus is significantly reduced in the intergrain regions. This is especially obvious between close grains that have an intergrain region of several nm. When the separation between adjacent grains is larger, for example at some of the triple-junctions, the elastic modulus is comparable to the values calculated on top of the grains. This indicates that, in these large intergrain regions, the probe may actually contact a grain beneath the adjacent set. An increase in the elastic modulus of these undergrains could be a result of the compressive stress exerted by the upper ones.

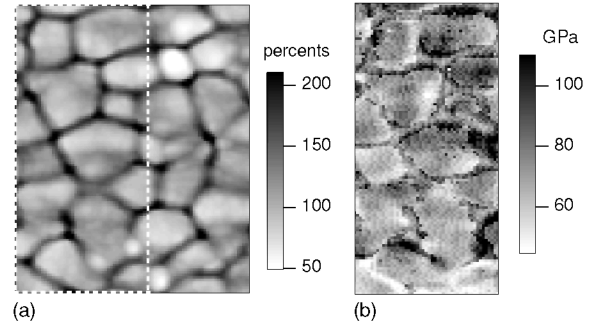

FIGURE 4. (a) Reconstructed contact area between the AFM probe and the topography shown in Fig. 1(a). The values are normalized to the contact area that the same AFM probe would experience on a flat surface; (b) Within the rectangular frame highlighted in (a) the indentation modulus has been calculated.

For the grain region as a whole, better correlations can be observed between the calculated map of the elastic modulus and the measured contact resonance frequency rather than with the topography. In topography, the grains look round and smooth but exhibit contrast in the contact resonance frequency. This is essentially due to the local change in the elasticity at the grain level and affects both the contact area and elastic modulus. Thus, even if on top of the grains the contact is essentially single-asperity, the contact area and elastic modulus are morphologically correlated and variations occur on every grain.

From Fig. 4(b), the indentation modulus over the grains is calculated to be (75 $\pm$ 10) GPa, comparable to the value obtained from indentation on Au surfaces [21]. Overall our measurements show a softening in the elastic response of the Au grains compared to the calculated

indentation modulus for single-crystal Au (111) and Au (001), which are 100 GPa and 90 GPa [19], respectively. Similarly, but at the microscale, local elastic softening of metallic grains has been recently measured on polycrystalline copper by resonance ultrasound microscopy [6].

In this work we have considered the effect of topography in extracting the indentation modulus from AFAM measurements on granular Au films. The analysis can be extended to other nano-size structured materials where consideration of topography-induced artifacts is necessary. Both topography and contact stiffness scans have to be combined for a correct measurement interpretation.

ACKNOWLEDGMENTS

We gratefully thank Dan Josell (NIST, Metallurgy Division) for providing the granular Au films.

REFERENCES

1. H. G. Craighead, *Science* **290**, 1532–1535 (2000).
2. R. E. Miller and V. B. Shenoy, *Nanotechnology*, **11**, 139–147(2000).
3. G. -F. Wang, X. -Q. Feng, S. -W. Yu, and C. -W. Nan, *Mat. Sci. Engr.*, **A363**, 1–8(2003).
4. L. Lu, M. L. Sui, and K. Lu, *Science*, **287**, 1463–1466 (2000).
5. M. A. Haque and M. T. A. Saif, *PNAS*, **101**, 6335–6340(2004).
6. H. Ogi, M. Hirao, T. Tada, and J. Tian, *Phys. Rev. B*, **73**, 174107 (2006).
7. J. R. Greer and W. D. Nix, *Phys. Rev. B*, **73**, 245410 (2006).
8. J. Wang, J. Lian, J. R. Greer, W. D. Nix, and K. -S. Kim, *Acta Materialia*, **54**, 3973–3982(2006).
9. U. Rabe and W. Arnold, *Appl. Phys. Letters*, **64**, 1493–1495 (1994).
10. K. Yamanaka, H. Ogiso, and O. Kolosov, *Appl. Phys. Letters*, **64**, 178–180 (1994).
11. Certain commercial equipment, instruments, or materials are identified in this article to adequately specify the experimental procedure. Such identification is not intended to imply recommendation or endorsement by the National Institute of Standards and Technology, nor is it intended to imply that the materials or equipment identified are necessarily the best available for the purpose.
12. G. Stan and W. Price, *Rev. Sci. Instrum.*, **77**, 103707 (2006).
13. G. Palumbo, S. J. Thorpe, and K. T. Aust, *Scripta Metall. Mater.*, **24**, 1347–1350 (1990).
14. D. .C. Hurley, M. Kopycinska-Muller, A. B. Kos, and R. H. Geiss, *Meas. Sci. Technol.*, **16**, 2167–2172(2005).
15. D. Passeri, A. Bettucci, M. Germano, M. Rossi, A. Alippi, V. Sessa, A. Fiori, E. Tamburri, and M. L. Terranova, *Appl. Phys. Letters*, **88**, 121910 (2006).
16. U. rabe, S. Amelio, M. Kopycinska, S. Hirsekon, M. Kempf, M. Goken, and W. Arnold, *Surf. Interface. Anal.*, **33**, 65–70(2002).
17. U. Rabe, K. Janser, and W. Arnold, *Rev. Sci. Instrum.*, **67**, 3281–3293(1996).
18. K. L. Johnson, *Contact Mechanics*, Cambridge University Press, 1987, pp. 188–220.
19. J. J. Vlasaak and W. D. Nix, *J. Mech. Solids*, **42**, 1223–1245(1994).
20. J. A. Greenwood and J. B. P. Williamson, *Proc. Royal Soc.*, **A295**, 300–319 (1966).
21. J. D. Kiely and J. E. Houston, *Phys. Rev. B*, **57**, 12588–12594 (1998).